Coupled Elastic-Thermal Dynamics of Deployable Mesh Reflectors

H. Shi[1] and B. Yang[2]

University of Southern California, Los Angeles, California, 90089-1453

M. Thomson[3] and H. Fang[4]

Jet Propulsion Laboratory, California Institute of Technology, Pasadena, CA 91109

This paper presents a coupled elastic-thermal dynamic model and a quasi-static strategy on the analysis of the reflector dynamics in the space mission. The linearized model, its natural frequencies and mode shapes are then derived upon the nonlinear static equilibrium of the structure. The numerical example is provided to fully adapt the strategy and investigate the dynamic behaviors of the structure. Finally the proposed method is applied on the sample of the deployable mesh reflector and the simulation results are presented. The research work delivered in the paper will be used to design the feedback surface controller in future.

I. Introduction

IN the past decades, the large deployable mesh reflector has brought continuously interest in research and industry. It has been used in many different projects for very broad space applications, such as mobile communications, remote sensing, global broadcasting, satellite communications, and climate forecasting. While many successful researches [1 - 4] have been conducted on developing the deployable mesh reflectors, due to the higher and higher mission requirements from NASA and industry, the larger reflectors with smaller surface error are still in the urgent demand.

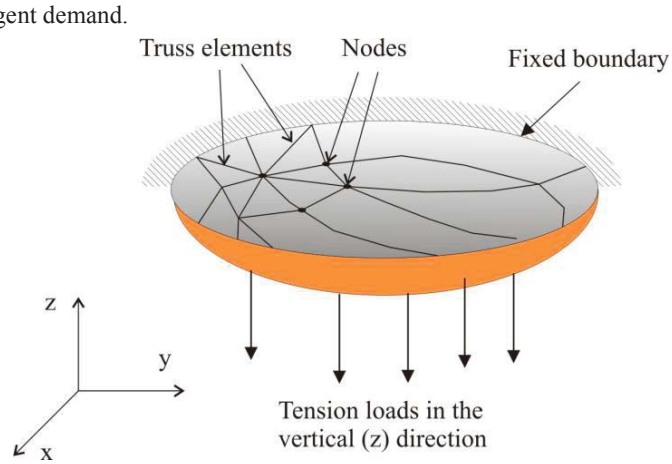

[1] Graduate Student, Dept. of Aerospace and Mechanical Engineering.

[2] Professor, Dept. of Aerospace and Mechanical Engineering. Email: bingen@usc.edu.

3 Principal Engineer, Mechanical Systems Engineering and Research Division, 4800 Oak Grove Drive, MS 299-100.

4 Technologist III, Mechanical Systems Engineering and Research Division, 4800 Oak Grove Drive, MS 299-100, Senior Member AIAA.

Figure 1. The deployable mesh reflector in consideration

Although it has been a challenge to increase both size and surface accuracy at the same time, the previous studies [5, 6] have suggested that the active control on the shape of structure should be introduced in the development of deployable space reflectors. To ultimately develop an active surface control technique, the authors' previous works have delivered an optimal design of initial profile and a nonlinear static model of mesh reflectors [7, 8]. The work in this paper is the continued research following the previous paper [9]. According to the structural dynamic theories [10 - 13], it is to analyze the dynamics of the mesh reflector in the space by considering the elastic-thermal properties and to serve the controller design purpose for improving the performance of the reflector's surface.

The mesh reflector structure discussed in this research is shown in Figure 1. The reflector has a fixed boundary outside and the working surface is constructed by the nodes and the truss elements. With the tension ties connecting to the nodes, the vertical external loads can be provided. In the second section of the paper, following the modeling formulation in Ref [9], a nonlinear model on coupled thermal-elastic dynamics is proposed. In the third section, the nonlinear model is linearized on the nonlinear static equilibrium and the dynamic properties are ready to obtain. In the fourth section, a quasi-static strategy is suggested for the analysis of in-space dynamics of reflectors. In the simulation and discussion section, the model and the strategy presented in the paper are implemented on two study cases, and the numerical results are presented before the paper is summarized and concluded.

II. A Nonlinear Model on Coupled Thermal-elastic Behavior

As it is mentioned above, besides investigating the nonlinear dynamic vibrations of structure, the dynamic distortion due to the temperature changes also need to be considered. To build up the model on the coupled thermal-elastic dynamics of the reflector, the model of single element is then first to discuss.

For a single truss element, the thermal strains ε_{therm} under temperature changes is defined as

$$\varepsilon_{therm} = \alpha \Delta T \tag{1}$$

where α is the thermal coefficient of the material. Then the total strain of kth element of the structure is the summary of thermal strain $\varepsilon_{therm,k}$ and elastic strain $\varepsilon_{elast,k}$ by assuming no expansions due to other factors such as piezoelectric effects, etc.:

$$\varepsilon_{t,k} = \frac{l_k - L_k}{L_k} = \varepsilon_{therm,k} + \varepsilon_{elast,k} \tag{2}$$

Due to the in-space working environments of the reflector, the gravity is the ignored and the potential energy all comes from the elastic energy of the material. Similar to the derivation in Ref. [9], the elastic energy of single element under thermal effects is

$$\begin{aligned} V &= \int_0^L \int_0^{\varepsilon} E_k\left(\varepsilon_{elast,k}\right)\varepsilon_{elast,k} A\left(\varepsilon_{t,k}, s\right) d\varepsilon_{elast,k} ds \\ &= \int_0^L \int_0^{\varepsilon_{t,k}-\varepsilon_{therm,k}} E_k\left(\varepsilon\right)\varepsilon A\left(\varepsilon + \varepsilon_{therm,k}, s\right) d\varepsilon ds \end{aligned} \tag{3}$$

with $E_k\left(\varepsilon_{elast,k}\right)$ to be Young's module and $A\left(\varepsilon_{t,k}, s\right)$ as the cross-section area at axial location s. If the same definitions of variables is used as in Ref. [9], such as $\left\{y_d\right\}_k$ to be the deformed nodal coordinates of the kth

element and $\{y_c\}_k$ is the deformed coordinates of center of mass in Eq. (4),

$$\{y_d\}_k = \{x_{i,d} \quad y_{i,d} \quad z_{i,d} \quad x_{j,d} \quad y_{j,d} \quad z_{j,d}\}^T \quad \{y_c\}_k = \{x_{c,k} \quad y_{c,k} \quad z_{c,k}\}^T \tag{4}$$

hence we have the variation of the elastic energy is

$$\delta V = \left(E_k\left(\varepsilon_{t,k} - \varepsilon_{therm,k}\right)\right)\left(\varepsilon_{t,k} - \varepsilon_{therm,k}\right)\int_0^L A\left(\varepsilon_{t,k}, s\right) ds \frac{\partial \varepsilon_{t,k}}{\partial \{y_d\}_k} \delta \{y_d\}_k \tag{5}$$

Adapting the assumption that each element has negligible moment of inertia and no damping effects within structure, the variation of the kinematic energy and virtual work are the same with the Eq. (16) and (17) in Ref. [9],

$$\delta T_k = -\delta \{y_d\}_k^T M_k \left[\frac{\partial \{y_c\}_k}{\partial \{y_d\}_k}\right]^T \{\ddot{y}_c\}_k \tag{6}$$

$$\delta W_{nc,k} = \delta \{y_d\}_k^T \{F_k\} \tag{7}$$

where M_k is the total mass of element, $\{F_k\}$ is the external force vector.

Applying extended Hamilton principle

$$\int_{T_1}^{T_2} \left(\delta W_{nc,k} - \delta V_k + \delta T_k\right) dt = 0 \tag{8}$$

the equation of motion for single element is

$$M_k \left[\frac{\partial \{y_c\}_k}{\partial \{y_d\}_k}\right]^T \{\ddot{y}_c\}_k + \left(E_k\left(\varepsilon_{t,k} - \varepsilon_{therm,k}\right)\right)\left(\varepsilon_{t,k} - \varepsilon_{therm,k}\right)\int_0^L A\left(\varepsilon_{t,k}, s\right) ds \left\{\frac{\partial \varepsilon_{t,k}}{\partial \{y_d\}_k}\right\}^T = \{F_k\} \tag{9}$$

Considering the whole structure, the variation of elastic energy is obtained from Eq. (4), as

$$\delta V = \sum_1^m \delta V_k = \delta \{y_{def}\}^T \sum_1^m \left\{\frac{\partial \varepsilon_{t,k}}{\partial \{y_{def}\}}\right\}^T \left(E_k\left(\varepsilon_{t,k} - \varepsilon_{therm,k}\right)\right)\left(\varepsilon_{t,k} - \varepsilon_{therm,k}\right)\int_0^L A\left(\varepsilon_{t,k}, s\right) ds \tag{10}$$

where $\{y_{def}\}$ is the global coordinate vector of all nodes. Therefore similar to the formulation in Ref. [9], the equation of motion under thermal load is written as

$$[M]\{\ddot{y}_{def}\} + \sum_1^m \left\{\frac{\partial \varepsilon_{t,k}}{\partial \{y_{def}\}}\right\}^T \left(E_k\left(\varepsilon_{t,k} - \varepsilon_{therm,k}\right)\right)\left(\varepsilon_{t,k} - \varepsilon_{therm,k}\right)\int_0^L A\left(\varepsilon_{t,k}, s\right) ds = \{Q\} \tag{11}$$

when $[M] = \left(\sum_1^m M_k [\gamma]_k^T [\gamma]_k\right)$, $[\gamma]_k = [\alpha]\frac{\partial \{y_d\}_k}{\partial \{y_{def}\}}$ and $\{Q\}$ is the external forces applied on the nodes.

III. Model Linearization

When developing the feedback controller, it is very common and useful to linearize the nonlinear model at the nonlinear static equilibriums. The static equilibrium of the model $\{\bar{y}_{def}\}$ can be obtained from Eq. (12) by

setting $\left\{\ddot{y}_{def}\right\}=0$ in Eq. (11),

$$\sum_{1}^{m}\left\{\frac{\partial\varepsilon_{t,k}}{\partial\left\{y_{def}\right\}}\right\}^{T}\left(E_k\left(\varepsilon_{t,k}-\varepsilon_{therm,k}\right)\right)\left(\varepsilon_{t,k}-\varepsilon_{therm,k}\right)\int_{0}^{L}A\left(\varepsilon_{t,k},s\right)ds=\left\{Q\right\} \tag{12}$$

In particular, considering the nonlinear equilibrium of a single element under the assumption of constant Young's module, uniform cross-section in geometry and negligible Poisson's effect, Eq. (12) can be rewritten as

$$\left\{\frac{\partial\varepsilon_{t,k}}{\partial\left\{y_d\right\}_k}\right\}^{T}E_k\left(\varepsilon_{t,k}-\varepsilon_{therm,k}\right)A_kL_k=\left\{F_k\right\} \tag{13}$$

From the elasticity theory,

$$\varepsilon_{t,k}=\frac{\sqrt{\left(x_{i,d}-x_{j,d}\right)^2+\left(y_{i,d}-y_{j,d}\right)^2+\left(z_{i,d}-z_{j,d}\right)^2}-L_k}{L_k} \tag{14}$$

then

$$\left\{\frac{\partial\varepsilon_k}{\partial\left\{y_{def}\right\}}\right\}^{T}=\frac{1}{L_k}\left[T_\beta\right]^T\begin{bmatrix}-1\\1\end{bmatrix} \tag{15}$$

with

$$\left[T_\beta\right]=\begin{bmatrix}\beta_x & \beta_y & \beta_z & 0 & 0 & 0\\ 0 & 0 & 0 & \beta_x & \beta_y & \beta_z\end{bmatrix},\quad \begin{aligned}\beta_x&=\frac{x_{j,d}-x_{i,d}}{l}\\ \beta_y&=\frac{y_{j,d}-y_{i,d}}{l}\\ \beta_z&=\frac{z_{j,d}-z_{i,d}}{l}\end{aligned},$$

$$\sqrt{\left(x_{i,d}-x_{j,d}\right)^2+\left(y_{i,d}-y_{j,d}\right)^2+\left(z_{i,d}-z_{j,d}\right)^2}=l$$

Substitute Eq. (15) into Eq. (12), we have

$$E_k\left(\varepsilon_{t,k}-\varepsilon_{therm,k}\right)A\left[T_\beta\right]^T\begin{bmatrix}-1\\1\end{bmatrix}=\left\{F_k\right\} \tag{16}$$

which is the same with the equilibrium equation of element in Ref. [8] and is a proof on the correctness of our nonlinear model. The nonlinear static equilibrium $\left\{\bar{y}_{def}\right\}$ can not be solved analytically in general, but the nonlinear solving algorithm proposed in the authors' previous work [8] is able to numerically solve the Eq. (12) in an accurate and efficient manner.

Since $\left\{y_{def}\right\}=\left\{\bar{y}_{def}\right\}+\left\{\Delta y_{def}\right\}$, according to the perturbation techniques, Eq. (11) can be linearized as

$$\left[M\right]\left\{\Delta\ddot{y}_{def}\right\}+\left[K_{therm}\right]\left\{\Delta y_{def}\right\}=\left\{P_{therm}\right\} \tag{17}$$

where

$$\left[K_{therm}\right]=\frac{\partial}{\partial\left\{y_{def}\right\}}\left(\sum\left(\left\{\frac{\partial\varepsilon_{t,k}}{\partial\left\{y_{def}\right\}}\right\}^{T}\left(E_k\left(\varepsilon_{t,k}-\varepsilon_{therm,k}\right)\right)\left(\varepsilon_{t,k}-\varepsilon_{therm,k}\right)\int_{0}^{L}A\left(\varepsilon_{t,k},s\right)ds\right)\right)\Bigg|_{\left\{\bar{y}_{def}\right\}} \tag{18}$$

$$\{P_{therm}\} = \{Q\} - -\left(\sum_{1}^{m} \left\{ \frac{\partial \varepsilon_{t,k}}{\partial \{y_{def}\}} \right\}^{T} \left(E_k \left(\varepsilon_{t,k} - \varepsilon_{therm,k} \right) \right) \left(\varepsilon_{t,k} - \varepsilon_{therm,k} \right) \int_{0}^{L} A\left(\varepsilon_{t,k}, s \right) ds \right) \Bigg|_{\{\bar{y}_{def}\}} \tag{19}$$

Comparing Eq. (11) , (17) with the models obtained in Ref [9] without any thermal effects, it can be seen that the coefficients of the second order derivative are the same, which reveals the fact that the thermal distortion does not affect the mass matrix.

Therefore the eigenvalue problem of the linearized model is to solve

$$\left(-\lambda_i [M] + [K_{therm}] \right) \{\mu\}_i = 0 \tag{20}$$

where $\{\mu\}_i$ is the eigenvector and the corresponding eigenvalue λ_i is obtained from

$$def\left([K_{therm}] - \lambda_i [M] \right) = 0 \tag{21}$$

Moreover, by adapting the analysis method in Ref [14], it is also able to indicate the ability to control the structure modes by different inputs. First rewrite the linear system Eq. (17) into the state space format,

$$\{\dot{x}\} = [A]\{x\} + [B]\{u\} \tag{22}$$

in which

$$\{x\} = \begin{Bmatrix} \{\Delta y_{def}\} \\ \{\Delta \dot{y}_{def}\} \end{Bmatrix}, \quad \{u\} = \{P_{therm}\}, \quad [A] = \begin{bmatrix} 0 & [I] \\ [M]^{-1}[K_{therm}] & 0 \end{bmatrix}, \quad [B] = [M]^{-1} \tag{23}$$

where $\{u\}$ is the vector of linearized external forces and is considered as the input of system. Define λ_{Ai} to be the *i*th eigenvalue of $[A]$ and the vector $\{B_j\}$ is the input direction vector corresponding to the *j*th input of $\{u\}$. Then for each λ_{Ai} and $\{B_j\}$, the matrix in (24) can be formulated and the minimum singular value $\underline{\sigma}_{ij}$ of each matrix will be calculated. Since $[A]$ can have many eigenvalues and the system may have multiple inputs, we can generate a 2-D table of the minimum singular values $\underline{\sigma}_{ij}$, in which one dimension is λ_{Ai} and the other one is the input element u_j. According to the reference [14], the minimum singular values in the table indicate how much influence the different inputs u_j have on controlling the different vibration modes of the structure.

$$\left[\lambda_{Ai}[I] - [A] \quad \{B_j\} \right] \tag{24}$$

IV. Quasi-static Strategy on the Space Mission

While the reflector is orbiting Earth in space, the amount of sunlight which shoots on the structure determines the surface temperature of the reflector. For one orbiting cycle, the range of the temperature variations could be from around 250K to 350K depending on the altitude of the different orbit, while the period time of each cycle varies from one hour to 24 hours. Therefore the speed of temperature variation is from around 0.004K/s to 0.07K/s, which can be considered very slow. By assuming the uniform temperature distribution on reflector elements, the temperature of the reflector gradually changes in a cycle and it is practicable and reasonable to treat the structural dynamic distortion under thermal variation as a quasi-static process. Hence, we propose the following strategy on the dynamic analysis of the deployable mesh reflector in space missions:

In the orbiting mission of the reflector, the dynamic thermal distortion is approximated as a quasi-static process. Each orbiting cycle is divided into multiple sections as each section experiences the same range of

temperature variation.

1) Static process:

Between different sections, the deformation of the reflector is treated in a purely static manner. Combining the deployment process, we further separate this static deformation into four steps which is shown in Figure 2. Before the reflector is deployed, it is folded in the spacecraft and has a virtual initial surface which the reflector will be deformed to under zero external forces. In this step, namely S_0, the reflector is in certain nominal temperature T_0 when no thermal distortion occurs at each element of structure. The optimal design approach of the initial profile of the reflector can be found in the authors' previous work [7].

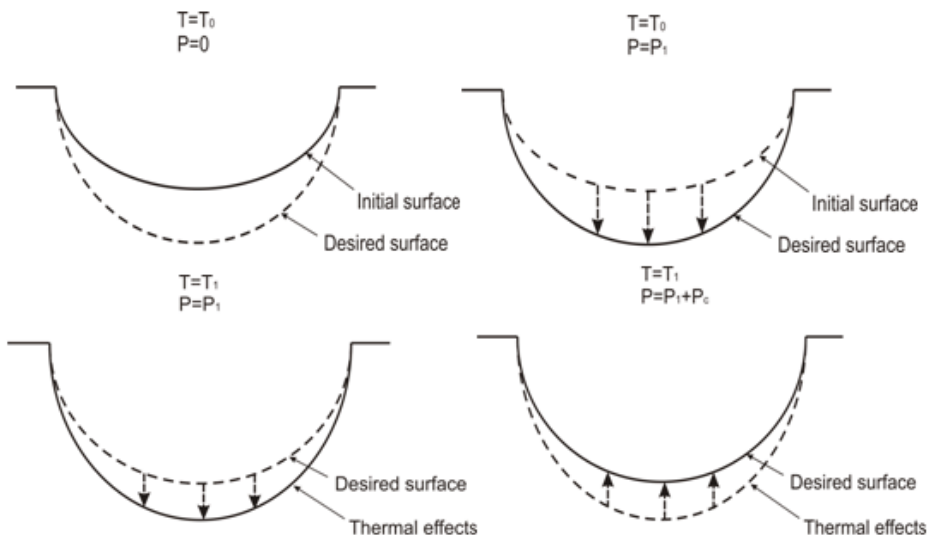

Figure 2. Static process of the quasi-static strategy.

Up-left: S_0; Up-right: S_1; Bottom-left: S_2; Bottom-right: S_3

In the step of S_1, which is the deployment process, the proper external forces P_1 which is predetermined, are applied on the nodes of the reflector and the deformation of the structure will generate the expected working surface. In this step, the reflector is still considered in the nominal temperature T_0.

However, as it is shown in the next step of S_2, the surface temperature T_1 determined by the space environment where the reflector is deployed and by Sun's ray on the surface, is always not the nominal temperature and the structure will statically distort under thermal loads into a new equilibrium with the external loads remain as P_1.

Finally, the external forces are adjusted in step of S_3 to ensure the surface of the reflector deforms back to the desired working shape under the current surface temperature T_1. It should be noticed that the nodal coordinates of this new working surface may not be the same with the nodal coordinates in the desired surface, but both surface share the exact same shape, which will maintain the surface performance unchanged as it is originally designed. The nonlinear static model and the solving method for S_1, S_2 and S_3 have been delivered in authors' previews research [8].

During the orbiting mission, the reflector will experience S_2 and S_3 each time it moves from one section to another. When entering the next section, the surface temperature of the reflector is considered to change into a new constant, such as T_1 and it will deform under the thermal effects. Then in the step of S_3, with proper additional forces P_c onto the previous loads P_1, the reflector deformed again and the surface is maintained in the designated shape.

2) Dynamic process:

Inside every section, the temperature is considered to remain constant. Therefore we only consider the dynamics of the reflector due to mechanical vibrations and disturbance, while the dynamic behavior due to the actual temperature changes is ignored. Upon the nonlinear static equilibrium of deformation within each section which is calculated above, the linearized model proposed in this paper is applied on the structure and the dynamic analysis such as the natural frequencies and mode shapes is investigated based on this linear model and will provide the important guidance for the further design of feedback surface controller.

V. Numerical Simulation and Discussion

In this section, a simulation for the deploying process and the orbiting mission is first carried out on a simple example of truss structure, which is also the guidance on the detailed procedure of the quasi-static strategy. Then the proposed strategy is applied on the sample of deployable mesh reflector with simulation results presented. In the first part, a simple truss is used as the study case and it has 6 nodes (3 are on the boundary) and 9 elements and the external forces are restricted in the vertical direction. Besides all the assumptions made in the section II and III, it is further assumed that each element has linear elasticity and uniform geometry along its axial direction without any Poisson's effect for simplicity. Moreover, in the initial shape of the structure no pre-tension occurs and each element is at its original length, as shown in Figure 3.

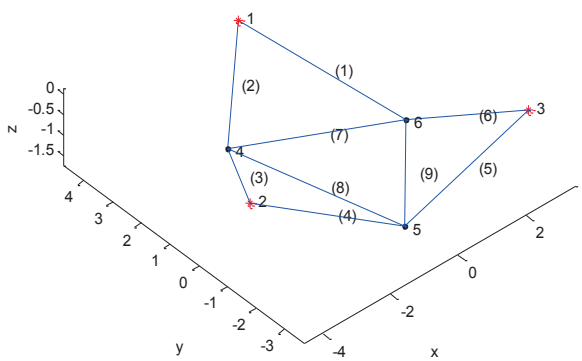

Figure 3. Initial shape of the example structure

A. Simulations on a simple example of truss structure

1) Static process of the strategy:

For the simple truss, the longitudinal rigidity EA of each element is 1000 N. With the nodes 1, 2, and 3 fixed on the boundary and nodes 4, 5, and 6 movable, the structure is designed to deploy to the a spherical working surface of diameter D = 5 m and height H = 3 m. The initial shape in figure 3 is treated as the status of the structure before deployment and the current surface temperature is set to be the nominal temperature. In steps of S_0 and S_1, once the structure is deployed into the space, the predetermined external forces, which are in the vertical down direction with magnitude of 10 N, are applied on nodes 4, 5, and 6 and generate the desired working shape. The nodal coordinates in initial and deformed shapes are displayed in the Table 1 and plotted in the Figure 4.

Table 1. Nodal coordinates in initial and deployed configurations

Node Number	Initial configuration (m)				Deployed configuration (m)		
	$x_{i,ini}$	$y_{i,ini}$	$z_{i,ini}$		$x_{i,def}$	$y_{i,def}$	$z_{i,def}$
1	0	4	0		0	4	0
2	-3.8730	-1	0		-3.8730	-1	0
3	2.8284	-2.8284	0		2.8284	-2.8284	0
4	-2.0241	1.9926	-0.9449		-2	2	-1.1231
5	-1.0017	-3.0220	-0.4362		-1	-3	-0.8729
6	1.9538	0.4781	-1.4283		2	0.5	-1.5552

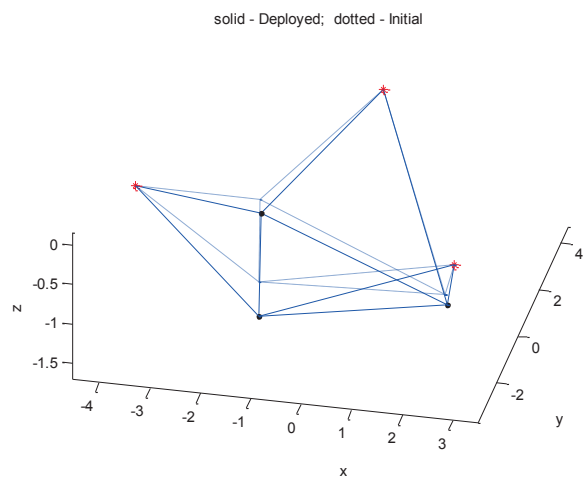

Figure 4. Initial and deployed shapes

When the temperature of the structure after deployment is 10 K higher than the nominal temperature, or in the case of the orbiting mission, when the structure enters the next section of period during the orbiting with 10 K of temperature increase at the surface, the structure will deform to another shape under the effects of static thermal distortion. To maintain the surface of the structure in the desired working shape against the thermal deformation, the external forces are adjusted statically, the structure is rebalanced into a new equilibrium and the surface deforms back to the designated shape. The above process is corresponding to the step of S_2 and S_3 , In the Table 2, the adjusted external loads, the nodal coordinates of the shape of thermal deformation and the rebalanced configuration are presented. Figure 5 shows the static shape deformation for these two steps. By comparing the nodal coordinates of rebalanced configuration in Table 2 with the deployed configuration in Table 1, it is confirmed that even though two surfaces are on the consistent working shape, the nodal coordinates are not necessarily the same.

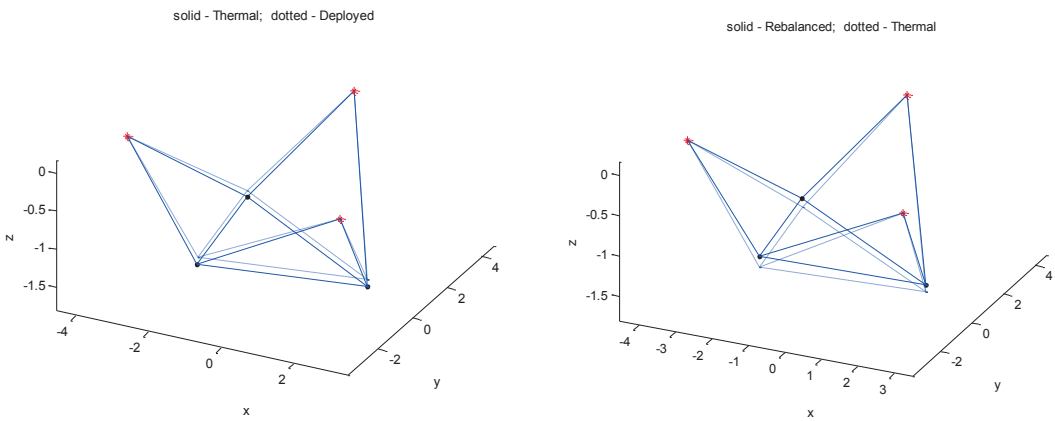

Figure 5. Static deformation process. *Left: Thermal deformation; Right: Rebalance deformation*

Table 2. From thermal deformation to rebalanced deformation

Node Number	Shape of thermal deformation (m)			Adjusted loads (N)	Rebalanced configuration (m)		
	$x_{i,ini}$	$y_{i,ini}$	$z_{i,ini}$		$x_{i,def}$	$y_{i,def}$	$z_{i,def}$
1	0	4	0	N/A	0	4	0
2	-3.8730	-1	0	N/A	-3.8730	-1	0
3	2.8284	-2.8284	0	N/A	2.8284	-2.8284	0
4	-2.0163	2.0198	-1.2012	-19.7582	-2.0265	2.0161	-1.1022
5	-1.0124	-3.0341	-0.9576	-18.5886	-1.0138	-3.0470	-0.8324
6	2.0203	0.5014	-1.6432	-13.1722	2.0135	0.5022	-1.5490

2) Dynamic process of the strategy:

As the structure is rebalanced to the desired shape, the nonlinear dynamic model is applied on the structure and is then linearized by Eq. (17) at the rebalanced equilibrium. Hence, the natural frequencies and mode shapes are calculated by Eq. (20) and (21); all natural frequencies and first three mode shapes are presented below:

Table 3. Natural frequencies of linearized model

Mode	ω_i (rad/s)	Mode	ω_i (rad/s)	Mode	ω_i (rad/s)
λ_1	2.4323	λ_4	5.1705	λ_7	13.4770
λ_2	3.4226	λ_5	5.6653	λ_8	14.6022
λ_3	4.1855	λ_6	12.3475	λ_9	15.5461

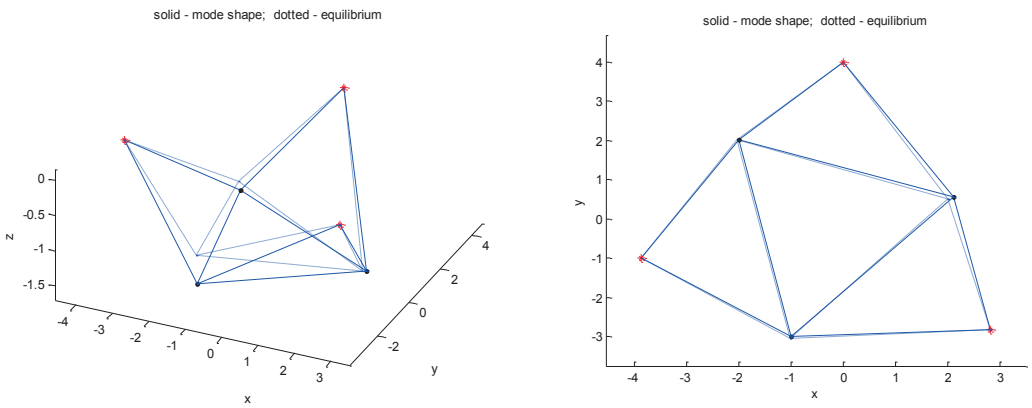

Figure 6. Mode shape 1 with structure equilibrium. *Left: 3-D view; Right: Top view*

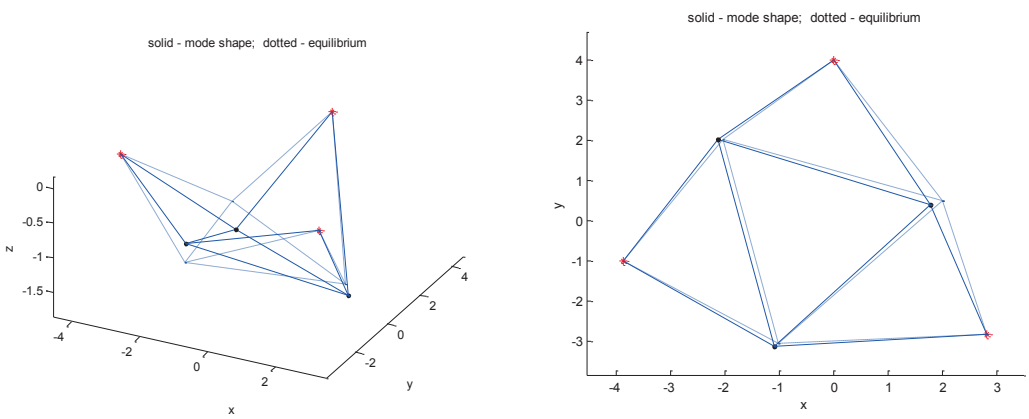

Figure 7. Mode shape 2 with structure equilibrium. *Left: 3-D view; Right: Top view*

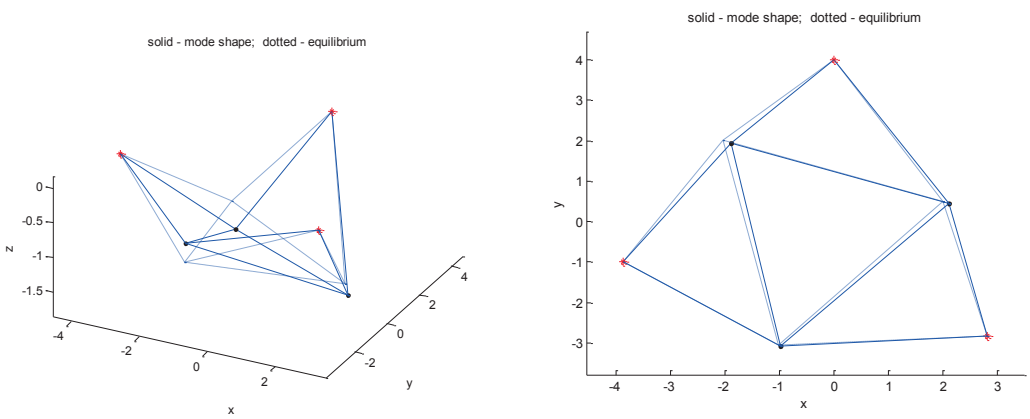

Figure 8. Mode shape 3 with structure equilibrium. *Left: 3-D view; Right: Top view*

Also by calculating the minimum singular values of the matrix in (24) for each input and every mode, a table of the singular values is obtained and only the results for the first three modes are shown below. From the Table 4, it can be concluded that the second input of the system which is the vertical load at node 5, has the largest influence when controlling the first mode of the structure at the current equilibrium. Similarly, for the second mode and third mode, the third input (the load at node 6) and the first input (the load at node 4) have most

control impact respectively.

Table 4. Influence of inputs on modes

	System input element		
Mode	u_1	u_2	u_3
λ_1	0.0193	0.0650	0.0003
λ_2	0.0029	0.0005	0.0439
λ_3	0.0436	0.0318	0.0160

B. Simulations on the sample of the deployable mesh reflector

Now the quasi-static strategy in the paper is applied on the sample of the deployable mesh reflector in Figure 9. It has 37 nodes, 90 members and a spherical working shape with diameter D = 30 m and height H = 11.18 m under proper vertical external loads which are predetermined. The element of the structure has the nonlinear longitudinal rigidity defined in Eq. (25) and the Poisson's effect is ignored. In the simulation, EA_0 is assigned to be 1.1121e+005 N.

$$EA(\varepsilon) = \begin{cases} EA_0 & \varepsilon > 0 \\ 0 & \varepsilon \le 0 \end{cases} \tag{25}$$

Following the similar procedure above for the simple example, the reflector is first deployed into the working surface from the initial shape. When the surface temperature of the reflector after deployment is not the nominal temperature, the structure will deform under thermal distortion. Also when the structure travels between different predetermined sections of the orbiting cycle, the surface of the reflector generates a new equilibrium under thermal effects. Finally the external loads are adjusted, the structure is rebalanced and the surface of the reflector is pulled back to the desired working shape. Hence in summary, for the static process in our strategy, there are four configurations of the reflector: initial, deployed, thermally deformed and rebalanced one. Due to the small thermal coefficient of the material and the large Young's modular, the nodal displacements between all four configurations are too small to be observed from figures and they all seem to be equal. Therefore, instead of showing the data sheet and the shape plots, the external forces for different steps of the static process are presented in the Table 5. Note that some external forces are repeated on different nodes due to the symmetry of the structure and only the distinct loads with relevant nodes are shown in the table. It can be seen that after rebalancing the reflector to ensure the surface in the desired working shape, the vertical external forces are increased and the elements of the structure are further tightened.

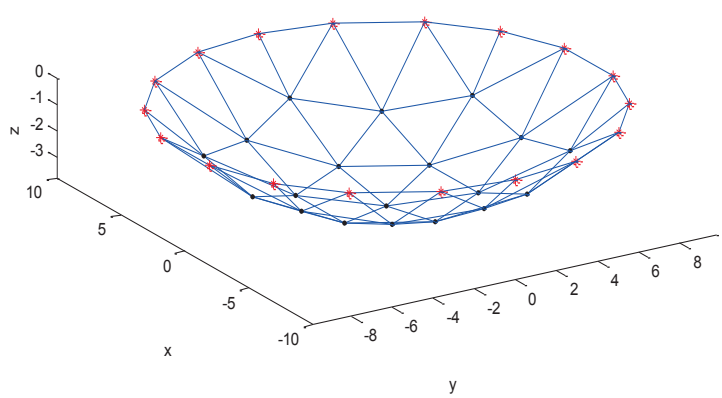

Figure 9. The sample of mesh reflector

Table 5. External forces in different equilibriums

Node Number	External forces in S_1 and S_2 (N)	External forces in S_3 (N)
1	-6.7799	-14.5709
2, 3, 4, 5, 6, 7	-7.3163	-15.7293
8,10,12,14,16,18	-8.6915	-18.7904
9,11,13,15,17,19	-8.6797	-18.7177

Since the reflector has been statically pulled back to the working shape by the tension ties under the temperature variation, the dynamics of the structure inside the section should be investigated. The nonlinear dynamic model (11) is applied and linearized at the nonlinear static equilibrium after the rebalanced deformation. Then from Eq. (20) and (21), the natural frequencies and mode shapes are calculated. The range of ω_i is from 13.66584 *rad/s* to 195.6173 *rad/s* and the first three distinct natural frequencies are shown below with relative mode shapes plotted in Figure 10.

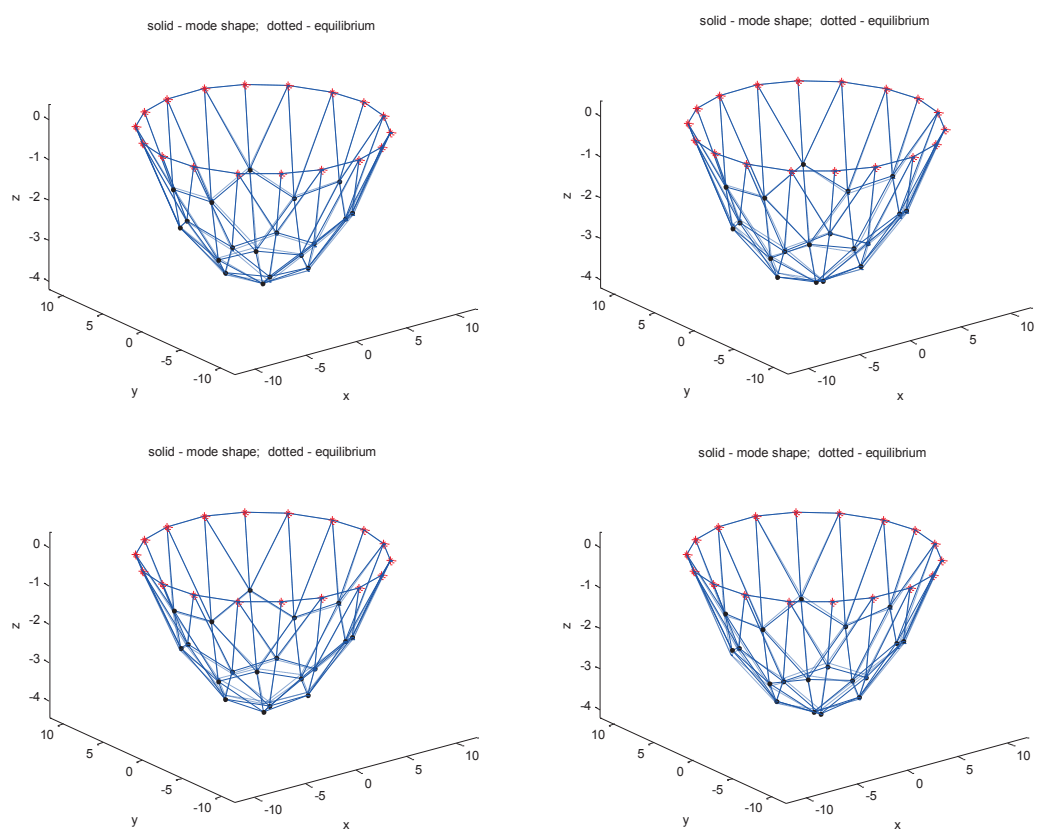

Figure 10. First four modes of the mesh reflector. *First: up-left; Second: up-right; Third: bottom-left; Forth: bottom-right*

$$\omega_{1,2} = 13.6584 \text{ rad/s} \quad \omega_3 = 14.7843 \text{ rad/s} \quad \omega_4 = 16.0913 \text{ rad/s}$$

Besides the analysis for the control impact of inputs on different dynamic modes as we did for previous example, it is very important to investigate the relationship between the natural frequencies of the linearized model and the variations of the parameters, such as the temperature of the reflector surface. Each time as the temperature varies, we need to consider two different static status of the reflector: S_2, when the structure is distorted away from the working surface under temperature changes; S_3, when the structure is rebalanced by the external loads under thermal effects and the working shape of the surface is maintained. Then based on these two nonlinear static equilibriums, the linearized models can be derived and the natural frequencies are calculated. Considering the overall range of temperature variation to be 100 K , the dynamics of the structure is analyzed for every 5 K changes of temperature and the results are plotted in Figure 11 and 12. In Figure 11, it indicates that naturally the natural frequencies of the system will increase when the temperature of the structure increases and this increasing curve may not be smooth. However, Figure 12 shows that after the structure is rebalanced to the working shape at each equilibrium, the natural frequencies decrease smoothly when the structure temperature increases.

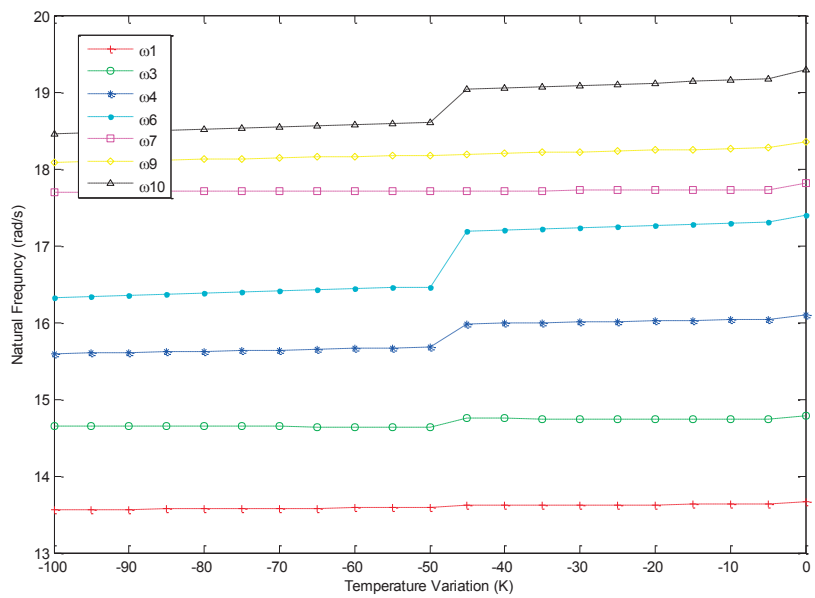

Figure 11. Variation of natural frequencies at S_2 status

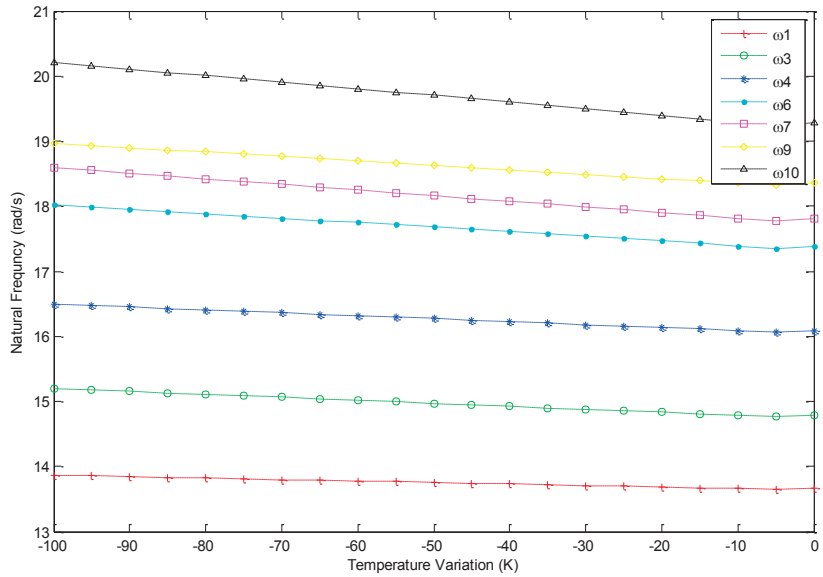

Figure 12. Variation of natural frequencies at S_3 status

VI. Conclusion

This study proposes a quasi-static strategy to analyze the dynamics of the deployable mesh reflector in the space mission based on a coupled thermal-elastic dynamic model which is highly control-orientated. The numerical example shown in the paper provides the detailed guidance on the procedure of modeling and analysis of the reflector dynamics. The simulation on the sample of deployable mesh reflector is then presented with the discussion on the temperature dependence of the natural frequencies. The results in this research work reveal the important properties of the dynamics of the mesh reflector, and the proposed strategy and models are crucial and will be used to design the feedback control of the surface shape in the next stage of research.

Acknowledgments

The work was carried out at the Jet Propulsion Laboratory, California Institute of Technology and the University of Southern California under a contract with the National Aeronautics and Space Administration.

References

1 Thomson, M., AstroMesh™ Deployable Reflectors for Ku and Ka Band Commercial Satellites, *20th AIAA International Communication Satellite Systems Conference and Exhibit*, Montreal, Quebec, May 12-15, 2002

2 Im, E., Smith, E.A., Durden, S.L., Huang, J., Rahmat-Samii, Y., and Lou, M., Instrument Concept of NEXRAD In Space (NIS) – A Geostationary Radar For Hurricane Studies, Proceedings of Intl. *Geoscience and Remote Sensing Symposium*, Toulouse, France, 2003

3 Natori, M.C., Takano, T., Inoue, T., Noda, T., Design and Development of a Deployable Mesh Antenna for MUSES-B Spacecraft, *34th AIAA /ASME /ASCE /AHS /ASC Structures, Structural Dynamics and Materials Conference*, Apr. 19-22, La Jolla, California, 1993

4 Meguro A., Tsujihata, A., Hamamoto, N., The 13 m Aperture Space Antenna Reflectors For Engineering Test Satellite VIII, Antennas and Propagation Society International Symposium, IEEE, Vol. 3, pp. 1520-1523, Aug. 1999

5 Hedgepeth, J. M., Accuracy Potentials for Large Space Antenna Reflectors with Passive Structure, *Journal of Spacecraft and Rockets*, Vol. 19, No. 3 pp 211-217, 1982

6 Gawronski, W. K., *Advanced Structural Dynamics And Active Control Of Structures*, Springer, 2004

7 Yang, B., Shi, H., Thomson, M. and Fang, H, Optimal Mounting of Deployable Mesh Reflectors Via Static Modeling and Quadratic Programming, *50th AIAA/ASME/ASCE /AHS/ASC Structures, Structural Dynamics and Materials Conference*, Palm Spring, CA, May. 4-7, 2009

8 Shi, H., Yang, B., Thomson, M. and Fang, H., Nonlinear Modeling And Optimal Initial Profile Solution For Deployable Mesh Reflectors, *51th AIAA/ASME/ASCE /AHS/ASC Structures, Structural Dynamics and Materials Conference*, Orlando, FL, April. 13 - 16, 2010

9 Shi, H., Yang, B., Thomson, M. and Fang, H., A nonlinear dynamic model for deployable mesh reflectors, extended abstract, will appear in 52th AIAA/ASME/ASCE /AHS/ASC Structures, Structural Dynamics and Materials Conference, Denver, CO, April 4-7, 2011

10 Pai, P. F., *Highly Flexible Structures: Modeling, Computation, And Experimentation*, AIAA, 2007

11 Yang, B., *Stress, Strain, And Structural Dynamics*, Elsevier, 2005

12 Meirovitch, L., *Principles And Techniques Of Vibrations*, Prentice Hall, 1997

13 Nayfeh, A. H. and P. Frank Pai, *Linear And Nonlinear Structural Mechanics*, Wiley, 2004

14 Hamdan, A.M.A., An Investigation Of The Significance Of Singular Value Decomposition In Power System Dynamics, *Electrical Power and Energy Systems*, Vol. 21, pp. 417–424, 1999